Mechanism for selectivity-inactivation coupling in KcsA potassium channels

Wayland W. L. Cheng[a,1], Jason G. McCoy[b,1], Ameer N. Thompson[b], Colin G. Nichols[a,2], and Crina M. Nimigean[b,2]

[a]Department of Cell Biology and Physiology, Washington University School of Medicine, 660 South Euclid Avenue, St. Louis, MO 63110, and Center for Investigation of Membrane Excitability Diseases, Washington University School of Medicine, 660 South Euclid Avenue, St. Louis, MO 63110; and [b]Departments of Anesthesiology, Physiology and Biophysics, and Biochemistry, Weill Cornell Medical College, 1300 York Avenue, New York, NY 10021

Edited by Christopher Miller, Brandeis University, Waltham, MA, and approved February 9, 2011 (received for review September 22, 2010)

Structures of the prokaryotic K^+ channel, KcsA, highlight the role of the selectivity filter carbonyls from the GYG signature sequence in determining a highly selective pore, but channels displaying this sequence vary widely in their cation selectivity. Furthermore, variable selectivity can be found within the same channel during a process called C-type inactivation. We investigated the mechanism for changes in selectivity associated with inactivation in a model K^+ channel, KcsA. We found that E71A, a noninactivating KcsA mutant in which a hydrogen-bond behind the selectivity filter is disrupted, also displays decreased K^+ selectivity. In E71A channels, Na^+ permeates at higher rates as seen with $^{86}Rb^+$ and $^{22}Na^+$ flux measurements and analysis of intracellular Na^+ block. Crystal structures of E71A reveal that the selectivity filter no longer assumes the "collapsed," presumed inactivated, conformation in low K^+, but a "flipped" conformation, that is also observed in high K^+, high Na^+, and even Na^+ only conditions. The data reveal the importance of the E71-D80 interaction in both favoring inactivation and maintaining high K^+ selectivity. We propose a molecular mechanism by which inactivation and K^+ selectivity are linked, a mechanism that may also be at work in other channels containing the canonical GYG signature sequence.

Potassium (K^+) channels exhibit the remarkable feature of catalyzing rapid ion conduction while maintaining strong selectivity for K^+ over Na^+. The extensive K^+ channel superfamily contains many members that have different selectivities, ranging from nonselective cation channels to highly selective K^+ channels, yet containing the same canonical GYG sequence. These residues form the narrow selectivity filter, in which the backbone carbonyls are positioned to coordinate dehydrated potassium ions (1). These carbonyls are constrained by the surrounding protein structure, which forms an intricate network of hydrogen bonds and salt bridges. In inward rectifying potassium (Kir) channels, a key structural feature of this network is a salt bridge that forms a molecular "bowstring" (2) bridging the top and bottom of the selectivity filter loop (2, 3) (Fig. 1). Alterations in this salt bridge are known to disrupt selectivity (2, 4, 5); several mutations have dramatic effects on permeation, rendering the channel essentially nonselective and highly permeable to Na^+. It has also been proposed that members of one subgroup of this family, the HCN channels, are less K^+ selective because they lack this network of molecular restraints (6), but the relevance of this structural network for selectivity in channels other than inward rectifiers, as well as the mechanism responsible for variable selectivity, remains to be seen.

Furthermore, alterations in the equivalent salt bridge residues that affect selectivity in the Kir channel family also lead to the induction of a phenomenon similar to C-type inactivation in voltage-gated K^+ channels (7). There is also a correlation between C-type inactivation and ion selectivity in eukaryotic voltage-gated K^+ channels: *Shaker* channels and other Kv channels such as Kv2.1 show decreased K^+ and increased Na^+ permeability when progressing to a C-type inactivated state (8, 9). By contrast, Na^+ and even the large glucose-like molecule, N-methyl-d-glucamine (NMG), are permeable through open Kv3 channels or a Kv1.5 mutant (R487V) where C-type inactivation is reduced (10, 11). The mechanism by which changes in selectivity are brought about by C-type inactivation are as yet unknown.

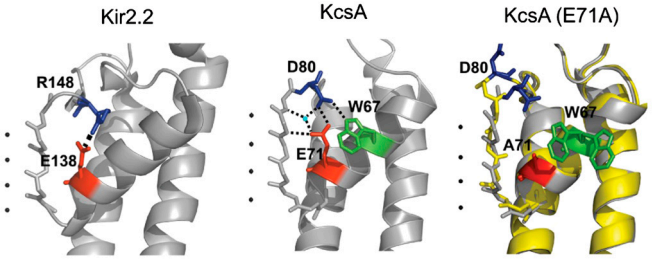

Fig. 1. The E71-D80 interaction is structurally analogous to the molecular bowstring in Kir channels and is disrupted in the E71A KcsA mutant. Images are taken from crystal structures of Kir2.2 (3JYC), KcsA (1K4C), and the flipped (yellow) and nonflipped (gray) structures of the E71A mutant of KcsA (1ZWI, 2ATK), showing the selectivity filter region from one subunit and highlighting the residues involved in a salt-bridge interaction in Kir2.2, and the hydrogen-bond interactions in KcsA. Black spheres represent potassium ions and the blue sphere represents water.

High-resolution structures of KcsA (12, 13) reveal that E71 and D80 form a hydrogen-bond interaction (14) at a similar location to the salt bridge in Kir channels (4) (Fig. 1). The E71A mutant that disrupts this bridge has been extensively studied to elucidate the mechanism of inactivation in KcsA, which is attributed to gating at the selectivity filter and likened to C-type inactivation in Kv channels (15–17). The E71A mutation abolishes pH-dependent inactivation, and the consequent high steady state open probability makes E71A a convenient model for electrophysiological studies (18–20). Given the similarity between the E71-D80 interaction in KcsA and the salt bridge in Kir channels, and the noninactivating phenotype of E71A, we questioned whether this mutation also alters selectivity of the channel. Molecular simulations show that the mutation changes the conformational dynamics and energy landscape of the selectivity filter (14, 16), and crystal structures of E71A in high concentrations of K^+ reveal two selectivity filter conformations: one that resembles the WT "conductive" structure (12) and a "flipped" structure showing outward movement of the D80 side chain along with distortion of carbonyls and changes in the location

Author contributions: W.W.L.C., J.G.M., C.G.N., and C.M.N. designed research; W.W.L.C., J.G.M., and A.N.T. performed research; W.W.L.C., J.G.M., A.N.T., C.G.N., and C.M.N. analyzed data; and W.W.L.C., J.G.M., C.G.N., and C.M.N. wrote the paper.

The authors declare no conflict of interest.

This article is a PNAS Direct Submission.

Data deposition: The crystallography, atomic coordinates, and structure factors have been deposited in the Protein Data Bank, www.pdb.org (PDB ID code 3OGC).

[1]W.W.L.C. and J.G.M. contributed equally to this work.

[2]To whom correspondence may be addressed. E-mail: cnichols@wustl.edu or crn2002@med.cornell.edu.

This article contains supporting information online at www.pnas.org/lookup/suppl/doi:10.1073/pnas.1014186108/-/DCSupplemental.

and occupancy of the ion binding sites (15) (Fig. 1). E71A channels show reduced affinity to extracellular TEA block and a pH-dependent increase in inward conductance compared to WT channels that may be related to the conformational changes in the "flipped" structure (21, 22). However, reversal potential shifts in biionic conditions suggest no significant change in selectivity for K^+ over Na^+ between E71A and WT KcsA (15, 23).

In the present study, we address the role of the E71-D80 interaction in ion selectivity. Using a radioactive flux assay, we show that E71A KcsA exhibits reduced selectivity for K^+ over Na^+ compared to WT, especially in the absence of K^+, where WT channels, but not E71A channels, become nonconductive. Also, single-channel recordings show enhanced relief of Na^+ block of K^+ conductance at depolarized potentials. The striking conclusion that disruption of the E71-D80 interaction in E71A KcsA results in reduced cation selectivity is supported by E71A KcsA crystal structures in the presence of high Na^+, which show that the E71A mutation not only prevents inactivation, but also prevents the collapse of the selectivity filter. These findings allow us to propose a molecular mechanism by which changes in selectivity are brought about by a process akin to C-type inactivation in eukaryotic K^+ channels.

Results

E71A KcsA Displays Altered K^+ Selectivity in $^{86}Rb^+$ Flux Assays. We examined selective permeation of E71A by assaying liposomal $^{86}Rb^+$ accumulation driven by different cations, as previously described for WT KcsA (24). At pH 7, K^+ drives $^{86}Rb^+$ uptake in both WT and E71A (Fig. 2*A*). However, although WT shows no detectable Na^+-driven $^{86}Rb^+$ uptake, E71A is clearly permeable to Na^+, which drives approximately 20% of the uptake driven by K^+ (Fig. 2*A*). The time course of K^+-driven uptake for E71A is much faster (>10×) than for WT at pH 4, and in order to rule out the possibility that the apparent increase in Na^+ permeation is simply proportional to the higher steady state open probability of E71A, pH was varied to make the rates of uptake comparable. At pH 8 for E71A and pH 4 for WT, the rate of K^+-driven uptake is nearly equivalent, but still only E71A shows measurable Na^+-driven $^{86}Rb^+$ uptake (Fig. 2*B*). $^{86}Rb^+$ flux through WT KcsA is undetectable when Na^+, Li^+, and NMG^+ are used to drive uptake, whereas Cs^+ and NH_4^+ show moderate uptake, consistent with previously published results (24) (Fig. 2*C*). By contrast, E71A shows significant $^{86}Rb^+$ uptake driven by Na^+, Li^+, Cs^+, and NH_4^+ (Fig. 2*C*), indicating a reduction of K^+ selectivity in E71A.

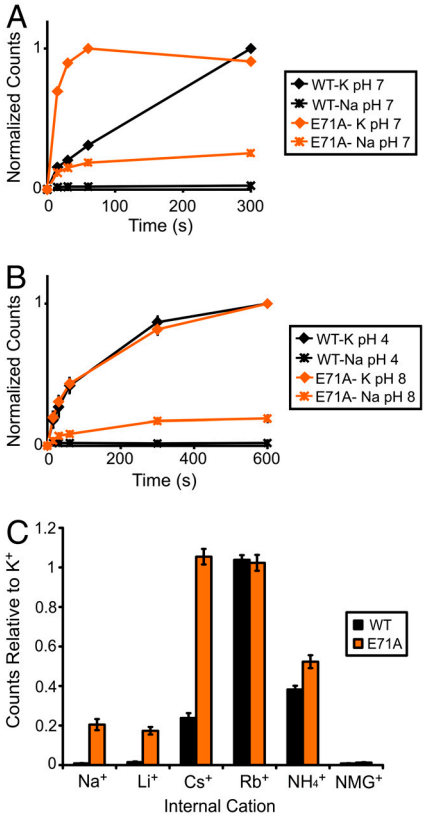

Fig. 2. The E71A KcsA mutant is more permeable to Na^+, Li^+, Cs^+, and NH_4^+. (*A*) Representative time courses of a liposomal $^{86}Rb^+$ flux assay of WT and E71A at pH 7 driven by intraliposomal K^+ or Na^+. Each time course is normalized to its own maximum level of uptake. (*B*) Same as *A* except assay performed at pH 4 for WT and pH 8 for E71A ($n = 4$, mean ± SEM). (*C*) Maximum $^{86}Rb^+$ uptake for WT and E71A at pH 7 driven by different intraliposomal cations and normalized to uptake driven by K^+ ($n = 5$, mean ± SEM).

E71A KcsA Displays Enhanced $^{22}Na^+$ Flux. To further examine Na^+ permeation, we extended the flux experiments to assay $^{22}Na^+$ accumulation. When K^+ is the intraliposomal cation, both WT and E71A show robust $^{22}Na^+$ uptake (Fig. 3 *A* and *B*) that is sensitive to block by Ba^+ (Fig. S1). The $^{22}Na^+$ flux is significantly slower than $^{86}Rb^+$ uptake under the same conditions for both channels. However, when Na^+ is the intraliposomal cation, WT shows no measurable $^{22}Na^+$ uptake, in stark contrast to E71A, which remains permeable to $^{22}Na^+$ (Fig. 3 *A* and *B*). These data indicate that WT KcsA becomes nonconductive in the absence of K^+, whereas E71A remains conductive and permeable to Na^+. In addition, E71A shows even more $^{22}Na^+$ uptake driven by Na^+ than driven by K^+ (Fig. 3*B*), suggesting that Na^+ permeation through E71A is actually inhibited by K^+, consistent with previous findings that the multiion configuration in the selectivity filter is an important determinant of selectivity in KcsA (25, 26).

Pronounced Relief of Na^+ Block at High Voltages in E71A KcsA. Although Na^+ shows increased permeability through E71A compared to WT, we were unable to obtain Na^+ currents in voltage-clamp recordings. It should be noted that, in the flux assay, a change in channel activity results in a change in both rate and

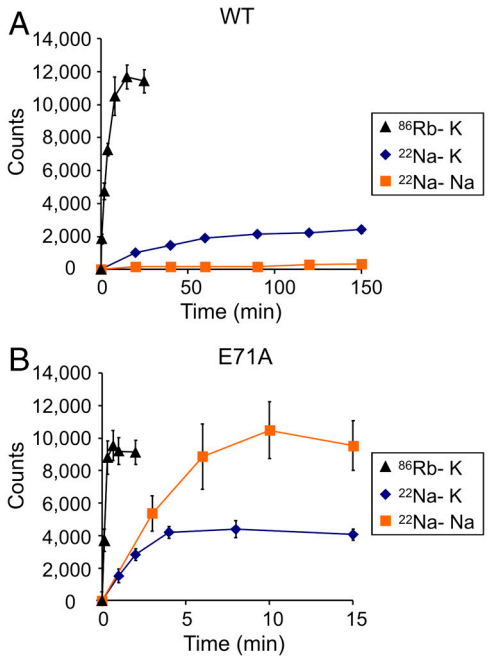

Fig. 3. WT KcsA, but not E71A, becomes nonconductive in the absence of K^+ and the presence of Na^+. (*A*) Time courses of WT fluxes at pH 7, showing K^+-driven $^{86}Rb^+$ uptake (black), K^+-driven $^{22}Na^+$ uptake (blue), and Na^+-driven $^{22}Na^+$ uptake (orange) ($n = 3$, mean ± SEM). (*B*) Same as *A* except for E71A ($n = 3$, mean ± SEM).

extent of uptake (27), such that we cannot directly assess permeability by measuring initial rates of radiotracer uptake (24), and the 20-fold slower rate of $^{22}Na^+$ uptake compared to $^{86}Rb^+$ in both WT and E71A (Fig. 3 *A* and *B*) is not simply indicative of a 20-fold lower Na^+/Rb^+ permeability ratio. To gain further insight to the Na^+ interaction with the pore, we examined intracellular Na^+ block of E71A and WT. Similar to its effects in WT KcsA (28), intracellular Na^+ modifies K^+ current through E71A KcsA by binding with very fast, unresolved kinetics in the inner cavity, thus reducing the apparent single-channel amplitude of the current in a voltage-dependent manner (Fig. 4 and Fig. S2). Although the current-voltage (IV) curve in the absence of Na^+ displays the expected monotonic increase with voltage, the Na^+-modified E71A IV curve is distinctly biphasic (Fig. 4*A*). Similar to WT, intracellular Na^+ causes a weak voltage-dependent block leading to a region of negative conductance [albeit less pronounced than in the WT channel (28)] in the 0 to 150–175-mV range. A Woodhull equilibrium block fit (29) (dashed blue line) yielded similar parameters as for the WT channel (Fig. 4, legend), suggesting that the cavity binding site for Na^+ is not different between WT and E71A. At the most positive voltages, the Na^+-modified current increases after a slight dip, almost parallel to the control (Fig. 4*A*). This "punch-through" region was previously interpreted as relief of block by Na^+ ions actually permeating through the selectivity filter (28). Na^+ begins to punch through the selectivity filter of E71A at a lower voltage than in the WT channel (approximately 175 mV compared to approximately 225 mV, Fig. 4*B*), and the resultant Na^+-modified current is significantly larger in E71A suggesting that Na^+ escapes through the selectivity filter with greater ease than in WT (Fig. 4*B*). We calculated an escape ratio (*SI Text*) to be between 6–10 ($k_2/b_2 > 6$); i.e., for each Na^+ ion escaping through the selectivity filter at high voltages there are at least 6 K^+ ions accompanying it. In contrast, the escape ratio previously obtained for WT KcsA channel was at least 30 K^+ ions permeating through the pore for each Na^+ ion ($k_2/b_2 > 30$) (28).

These data appear to contrast the findings of Cordero-Morales et al. (15) who suggested that K^+ selectivity was not reduced in E71A, based on extrapolated reversal potentials in biionic conditions. We repeated and extended those experiments by measuring reversal potentials in mixed K^+ and Na^+ conditions (see Fig. S3 and *SI Text*). Our data reveal no significant differences in reversal potentials between E71A and WT. However, in the presence of K^+, E71A is only slightly more permeable to Na^+ than WT based on $^{22}Na^+$ flux experiments (Fig. 3 *A* and *B*), and because the Na^+/K^+ permeability ratio for WT KcsA is estimated to be less than 0.006 (30) small differences in permeability ratios would not be detectable in this range.

Selectivity Filter of E71A Does Not Collapse in the Absence of K^+. To gain insight to the structural features underlying the selectivity differences between WT and E71A KcsA, we crystallized E71A in the absence of K^+ but in the presence of 150 mM NaCl (Table 1). Because of the relatively low resolution we took special precautions to verify that the final model, obtained by molecular replacement, was not biased by the starting model, as detailed in *Materials and Methods*, *SI Text*, and Figs. S4 and S5. Surprisingly, the resulting model has a selectivity filter (Fig. 5*A*) that looks very similar to that of a previously published E71A flipped structure solved in the presence of high K^+ [PDB ID code 2ATK (15)] (Fig. 5*C*, *Right*). Specifically D80, which was shown to coordinate E71 and W67 in the high-resolution WT KcsA structure [PDB ID code 1K4C (12)] (Fig. 5*B*, *Left*), is flipped such that the backbone atoms of residues 79, 80, and 81 are displaced by as much as 5 Å (Fig. 5 *A* and *C*, *Left*). In addition, the carbonyls in the selectivity filter are noticeably shifted from their positions in the WT structure, particularly that of V76, which is rotated almost 180° away from the pore. The atomic temperature factors in the filter region did not reflect a particularly higher flexibility than the remainder of the structure (Fig. S6). Importantly, our E71A KcsA structure in 150 mM Na^+ bears no resemblance to the collapsed, "nonconductive" low K^+ WT KcsA structure [PDB ID code 1K4D (12)] (compare Fig. 5 *A* and *B*, *Right*).

In contrast to the flipped high K^+ structure, where four K^+ ions were modeled in the S1 through S4 positions, in our flipped high Na^+ structure we observed electron density only in two locations, directly between the carbonyls of G77 and between the carbonyls of T75 (Fig. 5 *A* and *C*, *Right*). As the centers of the densities are relatively planar with the carbonyls, and the structures were obtained in high Na^+, they likely correspond to either Na^+ or water molecules. Regardless of the nature of these densities, the fact that we did not obtain the collapsed, putatively nonconductive filter structure (12) with E71A in the absence of K^+ (or in low K^+ and high Na^+; see Fig. S7 and Table S1) is consistent with the notion that the collapsed structure represents the inactivated state (17). Unlike the highly selective WT, E71A remains conductive and permeable to Na^+ in the absence of K^+ (Fig. 3).

Discussion

Role of the E71-D80 Interaction in Determining K^+-Dependent Cation Selectivity. The H-bond interaction between E71 and D80 in KcsA

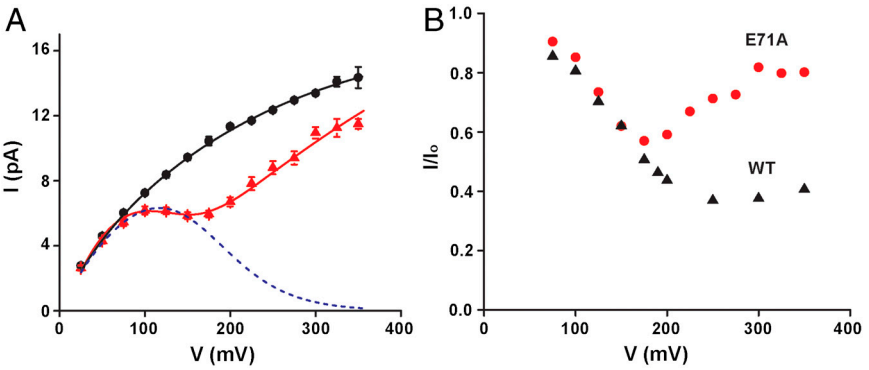

Fig. 4. Na^+ blocks E71A KcsA current in a voltage-dependent manner. (*A*) Open channel IV curves calculated from control (black circles, $n = 8$, mean ± SEM) and Na^+-blocked (red triangles, $n = 4$, mean ± SEM) single-channel currents. The curve through the control points is a hyperbolic fit with no theoretical significance. The dotted blue curve is a fit with Eq. **S1** with the fitted block parameters: $K_B(0) = 573$ mM and $Z = 0.64$ (compared with 500 mM and 0.55 for WT), and the smooth red line is a fit with the equation $I(V) = I_0(V)(1 + B/((1 + K/Q_K)(K_B + Q_B)))^{-1}$, where $K_B = K_B^{ap}(0)\exp(-zFV/RT)$ and Q_K and Q_B are Michaelis-type constants for K^+ and Na^+ (see ref. 28). Fitted parameters are as follows: Q_K is 6.1 $\exp(z_1FV/RT)$, where z_1 is 0.34, Q_B was set to 0.5 $\exp(-z_1FV/RT)$, and K_B is 283 $\exp(-z_2FV/RT)$, where z_2 is 0.9. (*B*) Plot of the ratio of Na^+-blocked and control currents (I/I_0) for E71A KcsA (red) and WT (black) showing the much larger increase in Na^+-modified E71A currents in the punch-through region.

Table 1. Data collection and refinement statistics

Data collection	E71A KcsA in high Na^+ and no K^+
Space group	I4
Cell dimensions	
a, *b*, *c* (Å)	154.90, 154.90, 75.49
α, β, γ (°)	90.0, 90.0, 90.0
Resolution (Å)	50.0–3.8 (3.89–3.80)*
R_{sym} or R_{merge}	10.7 (44.5)
$I/\sigma I$	11.9 (2.7)
Completeness (%)	99.8 (100.0)
Redundancy	3.6 (3.6)
Refinement	
Resolution (Å)	3.80
No. reflections	8449
R_{work}/R_{free}	24.9/28.4
No. atoms	
Protein	4070
Ligand/ion	2
Water	0
B factors	
Protein	79.5
Ligand/ion	19.6
rms deviations	
Bond lengths (Å)	0.005
Bond angles (°)	0.791

*Values in parentheses are for highest-resolution shell.

is structurally equivalent to the arginine-glutamate salt bridge in inward rectifiers that is an important molecular determinant of K^+ selectivity in these channels (2, 4, 5) (Fig. 1). The E71A mutation exhibits a noninactivating phenotype and has been used as a structural model of C-type inactivation (15, 16), for which there is a well-established connection with ion selectivity in Kv channels (8–11). However, despite marked structural changes in the E71A selectivity filter (15) (Fig. 1), the E71A mutation was not reported to significantly alter K^+ selectivity against Na^+ (15) (see Fig. S3). We show that in the absence of K^+, E71A is markedly more permeable to Na^+, Li^+, Cs^+, and NH_4^+ than WT KcsA (Fig. 2*C*). Flux assays can provide a more sensitive measure of permeability than reversal potential measurements when permeability ratios are low. Thus, in the presence of K^+, although reversal potentials are not measurably affected, E71A has reduced cation selectivity as detected by an increase in $^{22}Na^+$ flux (Fig. 3) and corroborated by punch through of blocking Na^+ ions (Fig. 4).

In the presence of Na^+ without K^+, KcsA WT exhibits a "second layer" of selectivity in which the filter adopts a collapsed, nonconductive filter and becomes impermeable to ions, including Na^+ (12, 31, 32). Our data provide functional correlates to this structural observation by demonstrating that in the absence of K^+, WT KcsA becomes nonconductive and impermeable to Na^+ (Fig. 3*A*). E71A, on the other hand, abolishes this second layer of selectivity (Fig. 3*B*), similar to a KcsA mutant in which G77 is replaced by D-Ala. In the absence of K^+, $KcsA^{D\text{-}Ala77}$ is permeable to Na^+ and does not show a collapsed filter (26). This suggests that E71A must maintain a conductive filter in the absence of K^+, and this is exactly what we observe in our K^+-deficient E71A structures, which show selectivity filters in an essentially identical conformation to the flipped E71A high K^+ structure (Fig. 5). Maintained pore conformation in zero K^+ has also recently been observed in the K^+ channel MthK and was attributed to differences between MthK and KcsA in the H-bond network behind the filter (32).

The functional difference between E71A and WT in the presence of ions other than K^+ is not just whether the WT channel is conductive or nonconductive. When $^{86}Rb^+$ uptake is driven by Cs^+ or NH_4^+, conductive WT channels show low, nonzero permeability to these ions but less so than E71A, especially in the case of Cs^+ (Fig. 2*C*). Taken together, our functional and

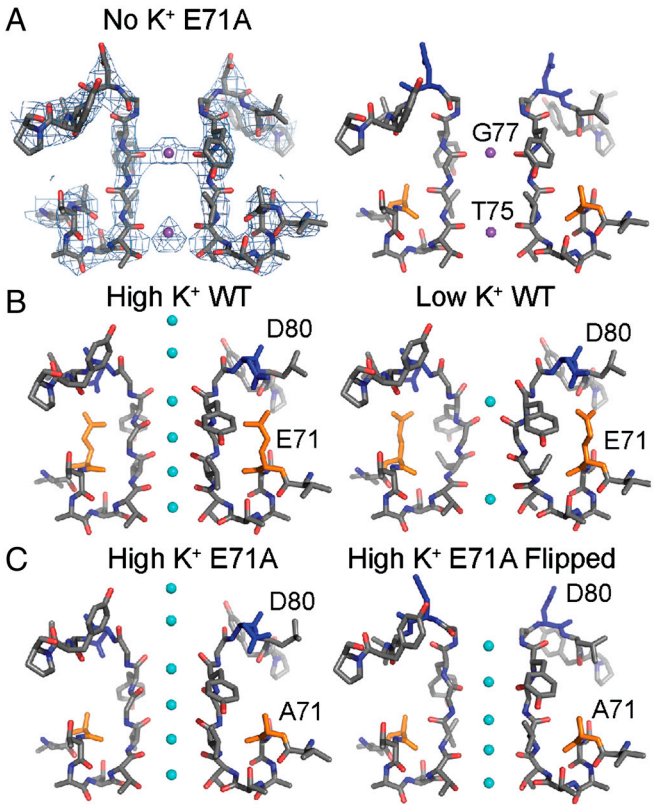

Fig. 5. Crystal structure of E71A KcsA features a noncollapsed selectivity filter. (*A*) Stick model of selectivity filter from E71A KcsA in the presence of 150 mM NaCl and the absence of K^+ and accompanying electron density (2Fo-Fc) contoured at 1.0σ. Residues G77 and T75 are labeled. For comparison, (*B*) stick models of filters of the conductive (*Left*) and collapsed (*Right*) states of WT KcsA [1K4C and 1K4D (12)]. (*C*) Stick models of filters of the nonflipped (*Left*) and flipped (*Right*) structures of E71A KcsA [2ATK and 1ZWI (15)]. Bound ions are purple (Na^+) or cyan (K^+) spheres.

structural data suggest that, in the absence of K^+, the E71A selectivity filter interacts with and responds to various cations differently than the WT channel, such that the mutant becomes more permeable to Cs^+, NH_4^+, Na^+, and Li^+. The low K^+ and no K^+ E71A structures indicate that, in the case of Na^+, this altered response is to maintain a conductive filter in the presence of Na^+ even with zero K^+.

Relationship Between the Nonconductive and the Inactivated State. Potassium or other permeant cations are cofactors for potassium channels, essential for maintaining their structure and function (33, 34). In *Shaker* channels, removal of all cations drives the channel into a dilated state with loss of selectivity, and ultimately into a long-lasting nonconductive state (35, 36). Interestingly, *Shaker* mutants that disrupt C-type inactivation are more resistant to becoming nonconductive (37). The relationship between permeation and C-type inactivation is also apparent from the fact that increased permeant ion concentrations slow C-type inactivation—an observation that is attributed to a "foot-in-the-door" mechanism (38, 39). It has been hypothesized that the collapsed low K^+ structure of KcsA is representative of a closed and potentially inactivated state (40, 41), and two recent, putative "open-inactivated" structures of KcsA (3F5W and 3F7V) (17) show selectivity filters that resemble the collapsed conformation of the low K^+ structure (12). Our results demonstrate that WT KcsA also enters a nonconductive state in the absence of K^+, in which it becomes very impermeable to Na^+ (Fig. 3*A*). E71A, a noninactivating mutant, is immune to this state. It remains permeable to Na^+ in the absence of K^+ (Fig. 3*B*), and the zero

K^+ structure of E71A reveals a presumably conductive selectivity filter (Fig. 5*A*). This suggests that the nonconductive state in KcsA is the inactivated state and supports the conclusion that the low K^+/high Na^+ collapsed structure of KcsA is representative of the inactivated filter structure (17). Our findings also suggest that the same structural forces that induce inactivation in KcsA (16), dependent on the E71-D80 interaction, are important for maintaining exquisite selectivity against Na^+ permeation in the absence of K^+.

Reduced Cation Selectivity of E71A in the Presence of K^+ and the Significance of the Flipped State in the E71A Structures. In addition to the marked differences between WT and E71A in the absence of K^+, E71A also shows reduced selectivity for K^+ over Na^+ in the presence of K^+, as evident in our $^{22}Na^+$ flux and Na^+ blocking punch-through experiments. E71A crystals obtained in high K^+ display both flipped and nonflipped conformations (15). Although the nonflipped structure resembles the WT high K^+ structures, there are notable differences in the position of the carbonyls and K^+ ion densities in the flipped E71A structure (15). We cannot exclude the possibility that the flipped conformation seen in E71A crystals grown in either high K^+ or high Na^+ is only infrequently encountered and that the nonflipped structure is the only relevant conformation during ion permeation. In this case, a decrease in selectivity when K^+ is present could result from perturbed electrostatics in the selectivity filter due to the neutralizing E71A mutation, affecting the balance between barrier heights and well depths, ultimately affecting selective permeation through the E71A KcsA pore. It seems reasonable to suggest, however, that the flipped selectivity filter conformation is actually yet another conductive filter state, encountered with high frequency during the normal E71A KcsA gating cycle. This state displays nonsubtly different cation binding sites, perhaps an indication that it may have different cation selectivity and be more permeable to Na^+ than the nonflipped filter structure. In support of this hypothesis, the only filter conformation encountered in our crystallization efforts of E71A in high Na^+ and either low (Fig. S6) or no K^+ was the flipped one (Fig. 5*A*).

We therefore propose a model in which E71A switches back and forth between the nonflipped (high K^+ selectivity) and the flipped (low K^+ selectivity) filter conformations (both conductive) during normal conduction. This would result in the channel being overall less K^+ selective than if the sole filter conformation during conduction were the nonflipped state. This model also predicts, in agreement with our $^{22}Na^+$ flux data (Fig. 3*B*), that in the presence of Na^+ and no K^+, the flipped, less K^+-selective filter conformation will be favored, making the channel even less selective than in the presence of K^+. The flipped state seen in E71A and not in WT KcsA may allow greater Na^+ permeation by either having lower energy barriers to Na entry/exit or by having a shallower binding site(s) for Na^+ in the filter (25).

Conclusions

The E71A mutation in KcsA not only reduces pH-dependent inactivation, but also reduces cation selectivity both in the absence and presence of K^+. In the absence of K^+, whereas WT KcsA becomes nonconductive, E71A remains conductive and permeable to Na^+. In the presence of K^+, E71A shows an increase in Na^+ permeability by $^{22}Na^+$ flux and Na^+ blocking punch-through experiments. The combination of our functional and structural results suggests two mechanisms whereby E71A reduces cation selectivity. In the absence of K^+, E71A prevents the selectivity filter from collapsing and favors a conductive, flipped filter conformation. In the presence of K^+, sampling of the flipped conformation facilitates Na^+ movement through the filter. Our findings suggest that the nonconductive selectivity filter associated with removal of permeant ions in KcsA is functionally and structurally similar to the inactivated state and offers a potential mechanistic explanation for correlated change in selectivity that can accompany C-type inactivation in eukaryotic potassium channels. Our results stress the importance of the scaffolding amino acid network behind the selectivity filter for modulating both cation selectivity and inactivation in channels with the same canonical GYG signature sequence.

Materials and Methods

Molecular Biology and Protein Purification. The E71A mutation was made using Quikchange Site-Directed Mutagenesis Kit (Stratagene) and confirmed by DNA sequencing. Protein for flux assays was produced as previously described (24) (42) and contained a C-terminal thrombin cleavage site and hexahistidine tag (LVPRGSHHHHHH) immediately after the KcsA gene, which was not cleaved. Protein for crystallography and Na^+ block assays was produced using JM83 *Escherichia coli* transformed with an N-terminal hexahistidine-tagged KcsA gene (with E71 mutated to A) in pASK90 (43) according to previous protocols (20). The histidine tag was located directly between methionine 1 and proline 2 of the protein sequence and was not cleaved.

Radioactive Isotope Flux Assay. 1-Palmitoyl-2-oleoyl-sn-glycero-3-phosphoethanolamine (POPE) and 1-palmitoyl-2-oleoyl-sn-glycero-3-phosphoglycerol (POPG) lipids and 4 μg of WT or E71A protein were solubilized in buffer A (450 mM XCl, where X is the test cation K^+, Na^+, Li^+, Cs^+, NH_4^+, Rb^+, or $NMGH^+$, 10 mM Hepes, 4 mM NMG, pH 7) with 35 mM CHAPS at 10 mg/mL. Liposomes were formed by spinning the protein/lipid sample through a partially dehydrated column of Sephadex G-50 beads, presoaked overnight in buffer A, to 2,500 rpm (Beckman TJ6). The sample was then spun through another column preequilibrated in buffer B (buffer A with 400 mM sorbitol instead of 450 mM XCl). Uptake was initiated by adding 400–600 μL of buffer B with 1–2 μL of $^{86}Rb^+$ or $^{22}Na^+$ (1 mCi/mL water), and aliquots flowed through Dowex cation exchange columns at desired time points, as described previously (44). Samples were counted in a scintillation counter.

Patch Clamping of Reconstituted Giant Liposomes. Giant liposomes were prepared as previously described (11). Liposomes were prepared as described for flux assay using 2 mg of lipids and 2 μg of KcsA, and centrifuged at 100,000 × *g* for 1 h at 4 °C (Beckman TL-100). The liposome pellet was resuspended in 5 μL of K-MOPS buffer, dried on a microscope slide as 2- to 3-μL spots, and rehydrated with 10 μL of K-MOPS buffer overnight at 4 °C. Patch-clamp recordings were performed with a K-succinate buffer in the bath (154 mM KCl, 10 mM succinate, pH 4), and the same buffer with varying concentrations of KCl and NaCl to make a total of 154 mM in the pipette (i.e., 54 mM KCl, 100 mM NaCl; 34 mM KCl, 120 mM NaCl; 14 mM KCl, 120 mM NaCl). KcsA, reconstituted in giant liposomes, is primarily oriented such that the intracellular side faces the bath in excised patch configuration (18). Because KcsA is blocked by Na^+ from the intracellular side (28), Na^+ was added only to the pipette. Membrane patches were voltage-clamped using an Axopatch 1-D amplifier, and currents were sampled at 3 kHz with low-pass filtering at 1 kHz. See *SI Text* for consideration of liquid junction potentials.

Single-Channel Lipid Bilayer Recording and Data Analysis. A horizontal planar bilayer system was used to incorporate channels and record currents (25, 30). The system contained two chambers separated by a partition containing a 100-μm diameter hole upon which a lipid bilayer (3:1 mass ratio of POPE and POPG solubilized in n decane) was formed. The *cis* chamber was filled with 90 mM KCl, 10 mM KOH, and 10 mM Hepes, pH 7. Under control conditions the *trans* chamber was filled with 90 mM KCl, 10 mM KOH, and 10 mM succinic acid, pH 4.0. To observe the effect of Na^+, a solution containing 10 mM NaCl, 90 mM KCl, 10 mM KOH, and 10 mM succinic acid, pH 4.0 was perfused into the *trans* chamber. An Axopatch 200 amplifier was used to record currents sampled at 20 kHz with low-pass filtering at 2 kHz. A description of the data analysis is provided in *SI Text* and Nimigean and Miller (28).

Crystallization and Structure Determination. Protein for crystallization was chymotrypsinized (Sigma), complexed with F_{AB} (12), purified via size exclusion chromatography, and dialyzed into 150 mM NaCl, 5 mM decyl maltoside (Anatrace), and 10 mM tris(hydroxymethyl)aminomethane pH 7.5, unless specified otherwise. Crystals were grown by the hanging drop vapor-diffusion method at 20 °C. The reservoir solution contained 20–23% (wt/vol) polyethylene glycol 400, 25–50 mM $MgSO_4$, and 100 mM MES pH 6.5. Cryoprotection was accomplished by increasing the polyethylene glycol 400 concentration in the reservoir to 40% (wt/vol) and then freezing the crystal in liquid N_2.

Crystals were screened and diffraction data collected at the Brookhaven National Laboratory on beamlines X25 and X6A. The data presented in Fig. 5 were collected at a wavelength of 1.10 Å and a temperature of 93 K. Reflections were indexed, integrated, and scaled using the HKL2000 package (45). The structure was solved by molecular replacement via molrep from the CCP4 suite of programs using the previously deposited E71A KcsA structure, 2ATK, as the initial model (46). Multiple starting models (2ATK, 1K4C, and 1K4D) were used to verify that model bias did not influence our final structure. Further discussion of the structure validation is provided in *SI Text* (also see Figs. S4 and Fig. S5). The structure was completed through multiple rounds of model building with Coot and refinement with REFMAC (47, 48). TLS groups were chosen based on the output of the TLSMD server (49).

ACKNOWLEDGMENTS. We thank Rick Jackimowicz and Jean Jakoncic for beamline support. We also thank D. E. Enkvetchakul for helpful discussions about the radioactive flux assay, M. A. Saquibal for protein production assistance, O. Boudker for advice with crystallography, and A. Accardi for critiquing the manuscript. Support is acknowledged from National Institute of Health Grants R01-HL54171 (to C.G.N.), R01-GM077560, and GM088352 (to C.M.N.), and Fellowships from the American Heart Association (0810196Z to W.W.C.) and from the National Science Foundation Graduate Research Fellowships Program (to A.N.T.). Use of the National Synchrotron Light Source, Brookhaven National Laboratory, was supported by the US Department of Energy, Office of Science, Office of Basic Energy Sciences, under Contract DE-AC02-98CH10886. Data for this study were measured at beamline X25 of the National Synchrotron Light Source, which is funded principally by the Offices of Biological and Environmental Research and of Basic Energy Sciences of the US Department of Energy and from the National Center for Research Resources of the National Institutes of Health; and beamline X6A, which is funded by the National Institute of Health under agreement GM-0080.

1. Doyle DA, et al. (1998) The structure of the potassium channel: Molecular basis of K^+ conduction and selectivity. *Science* 280:69–77.
2. Dibb KM, et al. (2003) Molecular basis of ion selectivity, block, and rectification of the inward rectifier Kir3.1/Kir3.4 K(+) channel. *J Biol Chem* 278:49537–49548.
3. Tao X, Avalos J, Chen J, MacKinnon R (2009) Crystal structure of the eukaryotic strong inward-rectifier K^+ channel Kir2.2 at 3.1 A resolution. *Science* 326:1668–1674.
4. Yang J, Yu M, Jan YN, Jan LY (1997) Stabilization of ion selectivity filter by pore loop ion pairs in an inwardly rectifying potassium channel. *Proc Natl Acad Sci USA* 94:1568–1572.
5. Sackin H, Nanazashvili M, Li H, Palmer L, Walters D (2010) A conserved arginine near the filter of Kir1.1 controls Rb/K selectivity. *Channels* 4:203–214.
6. Giorgetti A, Carloni P, Mistrik P, Torre V (2005) A homology model of the pore region of HCN channels. *Biophys J* 89:932–944.
7. Sackin H, Nanazashvili M, Li H, Palmer LG, Walters DE (2009) An intersubunit salt bridge near the selectivity filter stabilizes the active state of Kir1.1. *Biophys J* 97:1058–1066.
8. Starkus JG, Kuschel L, Rayner MD, Heinemann SH (1997) Ion conduction through C-type inactivated Shaker channels. *J Gen Physiol* 110:539–550.
9. Kiss L, LoTurco J, Korn SJ (1999) Contribution of the selectivity filter to inactivation in potassium channels. *Biophys J* 76:253–263.
10. Wang Z, Zhang X, Fedida D (2000) Regulation of transient Na^+ conductance by intra- and extracellular K^+ in the human delayed rectifier K^+ channel Kv1.5. *J Physiol* 523:575–591.
11. Wang Z, Wong N, Cheng Y, Kehl S, Fedida D (2009) Control of voltage-gated K^+ channel permeability to $NMDG^+$ by a residue at the outer pore. *J Gen Physiol* 133:361–374.
12. Zhou Y, Morais-Cabral JH, Kaufman A, MacKinnon R (2001) Chemistry of ion coordination and hydration revealed by a K^+ channel-Fab complex at 2.0 A resolution. *Nature* 414:43–48.
13. Morais-Cabral JH, Zhou Y, MacKinnon R (2001) Energetic optimization of ion conduction rate by the K^+ selectivity filter. *Nature* 414:37–42.
14. Berneche S, Roux B (2002) The ionization state and the conformation of Glu-71 in the KcsA K(+) channel. *Biophys J* 82:772–780.
15. Cordero-Morales JF, et al. (2006) Molecular determinants of gating at the potassium-channel selectivity filter. *Nat Struct Mol Biol* 13:311–318.
16. Cordero-Morales JF, et al. (2007) Molecular driving forces determining potassium channel slow inactivation. *Nat Struct Mol Biol* 14:1062–1069.
17. Cuello LG, Jogini V, Cortes DM, Perozo E (2010) Structural mechanism of C-type inactivation in K(+) channels. *Nature* 466:203–208.
18. Chakrapani S, Cordero-Morales JF, Perozo E (2007) A quantitative description of KcsA gating I: Macroscopic currents. *J Gen Physiol* 130:465–478.
19. Chakrapani S, Cordero-Morales JF, Perozo E (2007) A quantitative description of KcsA gating II: Single-channel currents. *J Gen Physiol* 130:479–496.
20. Thompson AN, Posson DJ, Parsa PV, Nimigean CM (2008) Molecular mechanism of pH sensing in KcsA potassium channels. *Proc Natl Acad Sci USA* 105:6900–6905.
21. Rotem D, Mason A, Bayley H (2010) Inactivation of the KcsA potassium channel explored with heterotetramers. *J Gen Physiol* 135:29–42.
22. Vales E, Raja M (2010) The "flipped" state in E71A-K^+-channel KcsA exclusively alters the channel gating properties by tetraethylammonium and phosphatidylglycerol. *J Membr Biol* 234:1–11.
23. Choi H, Heginbotham L (2004) Functional influence of the pore helix glutamate in the KcsA K^+ channel. *Biophys J* 86:2137–2144.
24. Heginbotham L, Kolmakova-Partensky L, Miller C (1998) Functional reconstitution of a prokaryotic K^+ channel. *J Gen Physiol* 111:741–749.
25. Thompson AN, et al. (2009) Mechanism of potassium-channel selectivity revealed by Na(+) and Li(+) binding sites within the KcsA pore. *Nat Struct Mol Biol* 16:1317–1324.
26. Valiyaveetil FI, Leonetti M, Muir TW, Mackinnon R (2006) Ion selectivity in a semisynthetic K^+ channel locked in the conductive conformation. *Science* 314:1004–1007.
27. Singh DK, Rosenhouse-Dantsker A, Nichols CG, Enkvetchakul D, Levitan I (2009) Direct regulation of prokaryotic Kir channel by cholesterol. *J Biol Chem* 284:30727–30736.
28. Nimigean CM, Miller C (2002) Na^+ block and permeation in a K^+ channel of known structure. *J Gen Physiol* 120:323–335.
29. Woodhull AM (1973) Ionic blockage of sodium channels in nerve. *J Gen Physiol* 61:687–708.
30. LeMasurier M, Heginbotham L, Miller C (2001) KcsA: It's a potassium channel. *J Gen Physiol* 118:303–314.
31. Gouaux E, Mackinnon R (2005) Principles of selective ion transport in channels and pumps. *Science* 310:1461–1465.
32. Ye S, Li Y, Jiang Y (2010) Novel insights into K^+ selectivity from high-resolution structures of an open K^+ channel pore. *Nat Struct Mol Biol* 17:1019–1023.
33. Krishnan MN, Bingham JP, Lee SH, Trombley P, Moczydlowski E (2005) Functional role and affinity of inorganic cations in stabilizing the tetrameric structure of the KcsA K^+ channel. *J Gen Physiol* 126:271–283.
34. Wang S, Alimi Y, Tong A, Nichols CG, Enkvetchakul D (2009) Differential roles of blocking ions in KirBac1.1 tetramer stability. *J Biol Chem* 284:2854–2860.
35. Gomez-Lagunas F (1997) Shaker B K^+ conductance in Na^+ solutions lacking K^+ ions: A remarkably stable non-conducting state produced by membrane depolarizations. *J Physiol* 499:3–15.
36. Loboda A, Melishchuk A, Armstrong C (2001) Dilated and defunct K channels in the absence of K^+. *Biophys J* 80:2704–2714.
37. Melishchuk A, Loboda A, Armstrong CM (1998) Loss of shaker K channel conductance in 0 K^+ solutions: Role of the voltage sensor. *Biophys J* 75:1828–1835.
38. Lopez-Barneo J, Hoshi T, Heinemann SH, Aldrich RW (1993) Effects of external cations and mutations in the pore region on C-type inactivation of Shaker potassium channels. *Receptors Channels* 1:61–71.
39. Baukrowitz T, Yellen G (1995) Modulation of K^+ current by frequency and external $[K^+]$: A tale of two inactivation mechanisms. *Neuron* 15:951–960.
40. Yellen G (2001) Keeping K^+ completely comfortable. *Nat Struct Biol* 8:1011–1013.
41. Domene C, Furini S (2009) Dynamics, energetics, and selectivity of the low-K^+ KcsA channel structure. *J Mol Biol* 389:637–645.
42. Enkvetchakul D, et al. (2004) Functional characterization of a prokaryotic Kir channel. *J Biol Chem* 279:47076–47080.
43. Skerra A (1994) Use of the tetracycline promoter for the tightly regulated production of a murine antibody fragment in Escherichia coli. *Gene* 151:131–135.
44. Nimigean CM (2006) A radioactive uptake assay to measure ion transport across ion channel-containing liposomes. *Nat Protoc* 1:1207–1212.
45. Otwinowski Z, Minor W (1997) Processing of X-ray diffraction data collected in oscillation mode. *Method Enzymol* 276:307–326.
46. Collaborative Computational Project N (1994) The CCP4 Suite: Programs for protein crystallography. *Acta Crystallogr D* 50:760–763.
47. Emsley P, Cowtan K (2004) Coot: Model-building tools for molecular graphics. *Acta Crystallogr D* 60:2126–2132.
48. Murshudov GN, Vagin AA, Dodson EJ (1997) Refinement of macromolecular structures by the maximum-likelihood method. *Acta Crystallogr D* 53:240–255.
49. Painter J, Merritt EA (2006) Optimal description of a protein structure in terms of multiple groups undergoing TLS motion. *Acta Crystallogr D* 62:439–450.